Journal of Drug Delivery Science and Technology 113 (2025) 107301

Contents lists available at ScienceDirect

Journal of Drug Delivery Science and Technology

journal homepage: www.elsevier.com/locate/jddst

Interferon gamma modifies nanoparticle tropism and cell uptake

Marius Remmert, Johannes Konrad, Jan Birringer, Achim Goepferich *

Department of Pharmaceutical Technology, University of Regensburg, Regensburg, Bavaria, 93053, Germany

ARTICLE INFO

Keywords:
Interferon-γ effect
Nanoparticle uptake
Nanoparticle tropism
Cholesterol content
Targeting efficiency

ABSTRACT

Interferon gamma (IFN-γ) challenges the ability of viruses to distinguish between target and off-target cells i.e. viral tropism. Due to the similarity of viruses and nanoparticles in shape and size, we hypothesized that the effect of IFN-γ on viruses also applies to virus-mimetic nanoparticles. Therefore, we determined the influence of IFN-γ on nanoparticle tropism and cell uptake. For our experiments, we used cyclic RGD-peptide (cRGD) functionalized polymeric nanoparticles and lipid nanocapsules (LNC) to target the $\alpha_v\beta_3$ integrin receptor on cell membranes of rat mesangial cells (rMCs), HeLa cells and human dermal microvascular endothelial cells (HDMEC). We used a nanoparticle concentration range between 0.1 and 2 nM. The IFN-γ concentrations and IFN-γ incubation times varied in the range of 100 IU–1000 IU and zero to 54 h respectively. When we measured nanoparticle uptake via flow cytometry 24 h after cytokine administration to cells, our findings confirmed that IFN-γ decreased the tropism as well as the uptake of functionalized nanoparticles by target cells. We were able to demonstrate a maximal IFN- γ effect at a concentration of 100 IU of IFN-γ and a 24-h incubation time. The presence of IFN-γ is associated with an upregulation of cholesterol 25-hydroxylase (CH25H). That the CH25H oxidation product, 25-hydroxycholesterol (25HC), is known to inhibit cell-nanoparticle interactions points at the potentially underlying mechanism of the observed INF-γ effect.

1. Introduction

Viruses are specialists in recognizing their target cells. Their ability to distinguish between target- and off-target cells is known as tropism [1–4]. Recently, various research groups used viral pathogens as blueprints for nanoparticle design. The strategy aims to mimic the stringent tropism of viruses. Thereby, side effects could be reduced since more nanoparticles reached their target tissue [5–9]. However, this concept often falls short of expectations in vivo. In tumor treatment, for instance, the proportion of nanoparticles reaching their target site is frequently found in the range between 1 % and 2.5 % percent [10] while the larger amount of an administered dose accumulates in off-target tissues. The great similarity between nanoparticles and viral pathogens in terms of size, shape and target cell specificity gave rise to our hypothesis that immune system effects on viral tropism might also affect nanoparticle biodistribution (tropism-transfer hypothesis). For instance, IFN-γ, known to diminish the tropism of several viral species [11–19], was previously shown to negatively affect target cell accumulation of nanoparticles in vitro [20]. To investigate this aspect further could be highly relevant for cancer therapy as tumors have increased IFN-γ concentrations compared to healthy tissues [21,22]. Therefore, drug nanotherapy could profit tremendously from a better understanding of IFN-γ effects on nanoparticle - cell interactions. We hypothesized that IFN-γ could reduce the uptake and tropism of nanoparticles which has a marked effect on drug nanotherapy for which target cell identification and cell uptake are essential. We assumed that the reason for the IFN-γ effect could be the altered cholesterol metabolism of cells. IFN-γ is known to increase the activity of CH25H, which in turn leads to an accumulation of 25HC in cell membranes [20]. At the same time, this leads to a cholesterol depletion of cell membranes, since 25HC stems from the hydroxylation of cholesterol.

To challenge our hypotheses, we first investigated the impact of IFN-γ on nanoparticle - cell interactions, which are of paramount importance for nanoparticle biodistribution. To this end, we examined the effect of IFN-γ on the uptake and tropism of nanoparticles for target and off-target cells. Rat mesangial cells (rMC) exhibit a larger quantity of $\alpha_v\beta_3$-integrin on their surface than HeLa cells [23]. Based on this difference, the uptake of cRGD nanoparticles into rMCs is enhanced compared to the uptake into HeLa cells. For our studies, we used (cRGD) functionalized nanoparticles that trigger clathrin-mediated endocytosis when binding to the $\alpha_v\beta_3$-integrin receptor. We investigated whether IFN-γ effects, such as a loss of nanoparticle tropism or the diminution of

* Corresponding author.
E-mail address: achim.goepferich@ur.de (A. Goepferich).

https://doi.org/10.1016/j.jddst.2025.107301
Received 3 April 2025; Received in revised form 14 July 2025; Accepted 18 July 2025
Available online 22 July 2025

particle uptake by target cells, depend on "cellular parameters" like cell type, IFN-γ incubation time and concentration or "particulate parameters" like receptor ligands in the nanoparticle corona, nanoparticle concentration and nanoparticle type. For our studies we used polymer nanoparticles consisting of poly (lactic-co-glycolic acid) (PLGA) and poly (lactic acid)-poly (ethylene glycol) (PLA-PEG) as well as LNCs, both functionalized with cRGD peptide tethered to 2 kDa PEG chains (PEG2k) for targeting the $\alpha_v\beta_3$ integrin subtype [24,25]. To determine the IFN-γ effect, we used flow cytometry and compared the cell uptake of cRGD-functionalized nanoparticles to ligand-free control nanoparticles in IFN-γ treated and untreated cells. To further scrutinize whether the nanoparticles were taken up by the cells or remained on the cell surface we used confocal microscopy which allowed us to localize particles during and after cell uptake.

2. Results

2.1. Nanoparticles

Lipid- and polymer nanoparticles could reproducibly be manufactured. Polymer nanoparticles had a size of 90 nm ± 20 nm, LNCs of 75 nm ± 20 nm. The zeta potential was between −25 and −45 mV for all particles. Booth nanoparticle types were stable in size and fluorescence properties for at least seven days (see supplementary information).

2.2. Determination of the IFN-γ effect in cell monoculture

Uptake of nanoparticles into the rMCs was measured via flow cytometry. Fig. 1 illustrates the cRGD functionalized polymer nanoparticles (cRGD-pNP), carboxylic acid group functionalized polymer nanoparticles (COOH-pNP) and uncharged methoxy group functionalized polymer nanoparticles (MeO- pNP) uptake by rMCs in the presence and absence of IFN-γ. COOH-pNP and MeO-pNP serve as control nanoparticles. The extent of cRGD-pNP uptake in untreated rMCs is significantly higher than the uptake of COOH-pNP (P value < 0.0001). The value of cRGD-pNP and MeO-pNP varies significantly between untreated and IFN-γ-treated cells. In the case of cells treated with IFN-γ, a slightly higher cRGD-pNP uptake relative to the COOH-pNP can be observed, although it is no longer significant. The decrease in the uptake of cRGD-pNP is much more pronounced compared to the MeO-pNP. In summary there is a significant IFN-γ effect in case of the cRGD-pNP and COOH-pNP uptake. Although the IFN-γ effect is not significant for the MeO-pNP, a trend of reduced uptake in the presence of IFN-γ can also be seen for these control nanoparticles. Overall, the reduced cell uptake is most pronounced for the cRGD-pNP, followed by the COOH-pNP and the MeO-pNP. This ranking holds also true for the nanoparticle uptake in the absence of the cytokine. The more nanoparticles are taken up into the cells, the greater is the reduction of nanoparticle uptake into target cells in the presence of IFN-γ. The effect is not only visible in the altered absolute nanoparticle uptake, but also in the loss of cRGD-pNP uptake relative to the COOH-pNP. The functionalization seems to provide no longer an uptake advantage compared to the control nanoparticles when the cytokine is present.

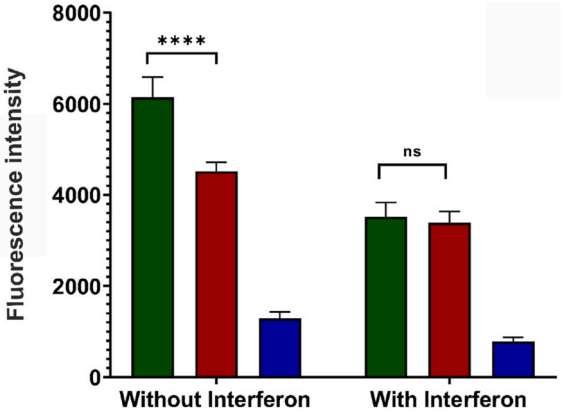

Fig. 1. IFN-γ effect on the uptake of cRGD-pNP (green bar), COOH-pNP (red bar) and MeO-pNP (blue bar) by rMCs. Quantity of endocytosed nanoparticles in the presence and absence of IFN-γ measured as APC-A geoMean fluorescence intensity [a.u.] in flow cytometry. Particle concentration was 2 nM, IFN-γ concentration was 100 IU and IFN-γ incubation time was 24 h **** = P value ≤ 0.0001; *** = P value ≤ 0.001; ** = P value ≤ 0,01; * = P value ≤ 0,05; ns = P value > 0,05.

2.3. The impact of nanoparticle concentration

We measured the cRGD-pNP and MeO-pNP uptake at four different nanoparticle concentrations of 2 nM (Fig. 2A), 1 nM (Figs. 2B), 0.5 nM (Figs. 2C) and 0.1 nM (Fig. 2B). The objective of this experiment was to scrutinize if the IFN-γ effect is dependent on nanoparticle concentration. Nanoparticle uptake was measured as cell fluorescence in the presence or absence of IFN-γ. The uptake of 2 nM, 1 nM and 0.5 nM cRGD-pNP is significantly reduced by the IFN-γ treatment while the uptake of 2 nM and 0.5 nM MeO-pNP does not change significantly (Fig. 2A). As expected, the total uptake of nanoparticles from the 0.1 nM solution is much lower than from higher concentrated solutions. However, the trend that the uptake of the cRGD-pNP changes significantly by pre-incubation with IFN-γ, while the uptake of the MeO-pNP does not change significantly, can also be seen with the 0.1 nM concentrated nanoparticles (Fig. 2D). The results reveal that the IFN-γ effect is not concentration-dependent and can therefore be analyzed regardless of the nanoparticle concentration used.

2.4. Impact of the cell line and the particle system on the reduced nanoparticle uptake caused by IFN-γ

To further verify the validity of our findings, we investigated whether an IFN-γ effect also occurs in other types of particle systems such as LNCs and other cells such as HDMECs. Following a 24-h incubation with IFN-γ we measured a diminished uptake of cRGD functionalized LNC nanoparticles (cRGD-LNC) in HDMECs. (Fig. 3A). The uptake of the methoxy group functionalized LNC nanoparticles (MeO-LNC) into the HDMECs was not affected. (Fig. 3A). Differences in uptake between the cRGD-LNC and the MeO-LNC were only significant in the absence of IFN-γ. Compared to untreated cells, IFN-γ treated HDMECs behave differently. In this case, there is no difference in the uptake of the cRGD-LNC and MeO-LNC. This means that the significant difference between the cRGD-LNC and MeO-LNC, which can be measured under untreated conditions is no longer present in IFN-γ treated cells. The uptake of cRGD-LNC into rMCs is considerably higher than the uptake into the HDMECs (Fig. 3B). cRGD-LNC were taken up to a significantly greater extent by the untreated rMCs compared to IFN-γ treated rMCs (Fig. 3B). Differences of the cRGD-LNC uptake ratio between untreated and IFN-γ treated cells is in case of the HDMESc much less pronounced compared to that of the rMCs. Overall, the impact of the IFN-γ treatment regarding the uptake into the rMCs is comparable between the cRGD-LNC and the cRGD-pNP (Figs. 1 and 3). It can, therefore, be concluded that the IFN-γ effect is strongly dependent on the cell line and less on the particle system.

2.5. Impact of IFN-γ on nanoparticle tropism and uptake in a rMC/HeLa cell co-culture

The diagrams in Fig. 4 show the nanoparticle uptake in cocultures of rMCs with HeLa cells in the presence and absence of IFN-γ. This experiment helps us to understand the impact of IFN-γ on the tropism of functionalized nanoparticles. Fig. 4A shows the uptake of nanoparticles into the target cells (rMC) of the co-culture. Differences in cell uptake of

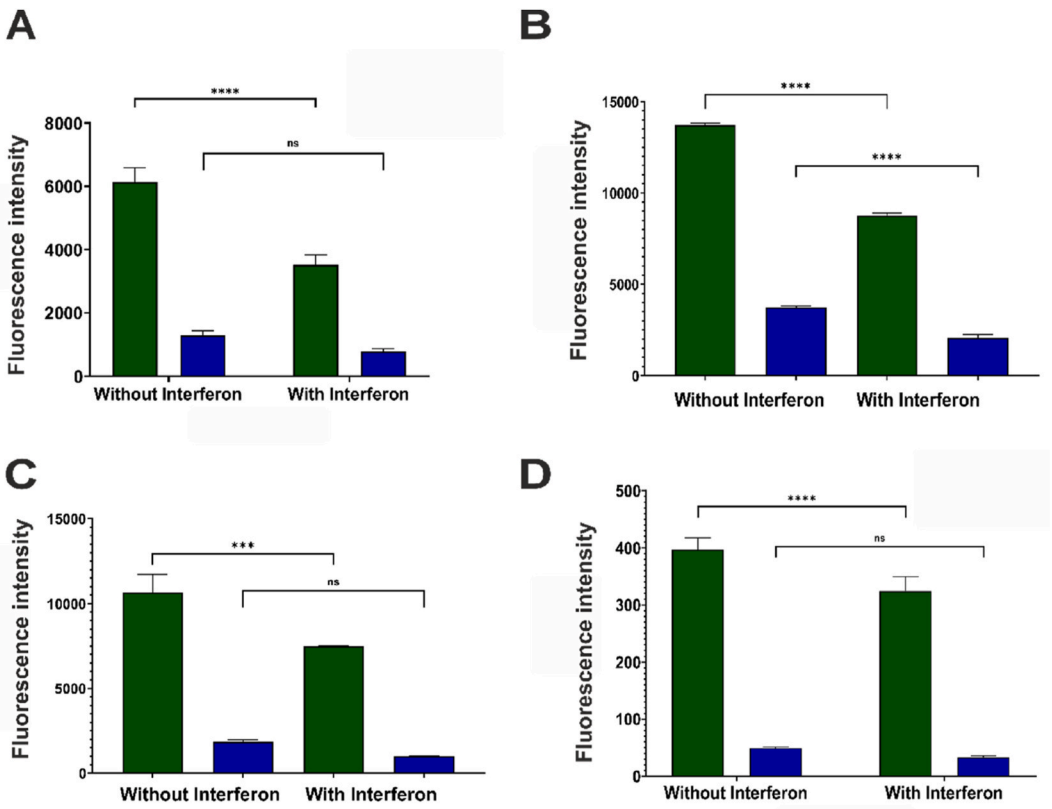

Fig. 2. Impact of particle concentration on the IFN-γ effect. Ordinate (APC-A geoMean fluorescence intensity [a.u.]): quantity of endocytosed nanoparticles (green: cRGD-pNP; red: MeO-pNP); Abscissa (treatment), The particle concentration was 2 nM (A), 1 nM (B), 0.5 nM (C) and 0.1 nM (D). IFN-γ concentration was 100 IU and IFN-γ incubation time was 24 h **** = P value ≤ 0.0001; *** = P value ≤ 0.001; ** = P value ≤ 0,01; * = P value ≤ 0,05; ns = P value > 0,05.

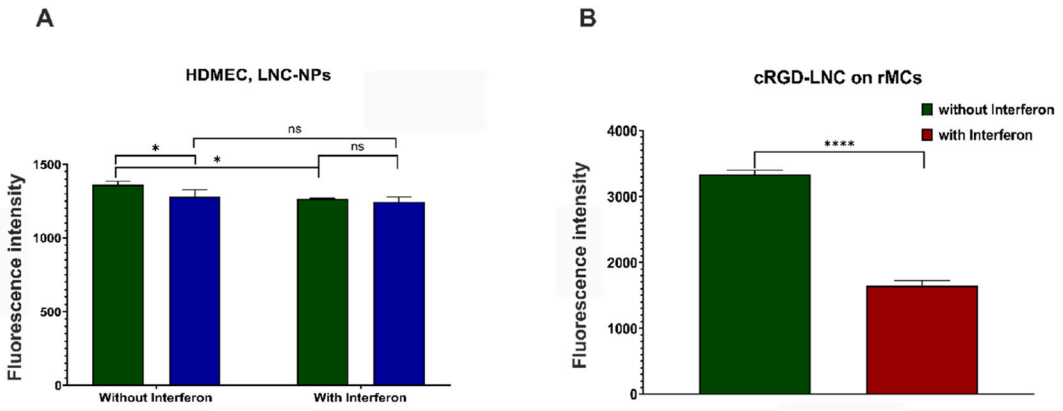

Fig. 3. IFN-γ effect on human dermal microvascular endothelial cells (HDMEC) compared to the IFN-γ effect on rMCs. Ordinate (FITC-A geoMean fluorescence intensity [a.u.]): quantity of endocytozed nanoparticles; Abscissa (treatment), The diagram shows the effect of IFN-γ on the uptake of cRGD-LNC (green bar) and MeO-LNC (blue bar) into HDMECs (A) or rMCs (B). Nanoparticle concentration was 2 nM, IFN-γ concentration was 100 IU and IFN-γ incubation time was 24 h **** = P value ≤ 0.0001; *** = P value ≤ 0.001; ** = P value ≤ 0,01; * = P value ≤ 0,05; ns = P value > 0,05.

cRGD-pNP, MeO-pNP and COOH-pNP in the presence and absence of IFN-γ is significant. Fig. 4B maps the uptake of polymer nanoparticles into the off-target cells (HeLa cells) of the co-culture. The quantity of nanoparticles taken up by off-target cells decreases from cRGD-pNP over COOH-pNP to MeO-pNP. IFN-γ has no effect on cell uptake. Differences between COOH-pNP, MeO-pNP and cRGD-pNP hardly changed after the 24 h IFN-γ preincubation. Evaluating the uptake of cRGD-pNP into target cells and off target cells of the co-culture, the difference in uptake of cRGD-pNP is highly significant in the untreated case. A significant difference in uptake quantity of cRGD-pNP occurs also in IFN-γ pretreated co-culture, even if it is not that pronounced. A significant alteration in uptake amount of cRGD-pNP into target cells of the co-culture can be measured. Uptake amount of cRGD-pNP into off-target cells of the co-culture is hardly and not significantly affected by an IFN-γ preincubation. We document a reduced uptake and a loss of tropism of cRGD-pNP in co-culture.

2.6. Verification of the localization of the nanoparticle in relation to the cells

Flow cytometry enables conclusions regarding the quantitative extent to which the measured cells are associated with nanoparticles.

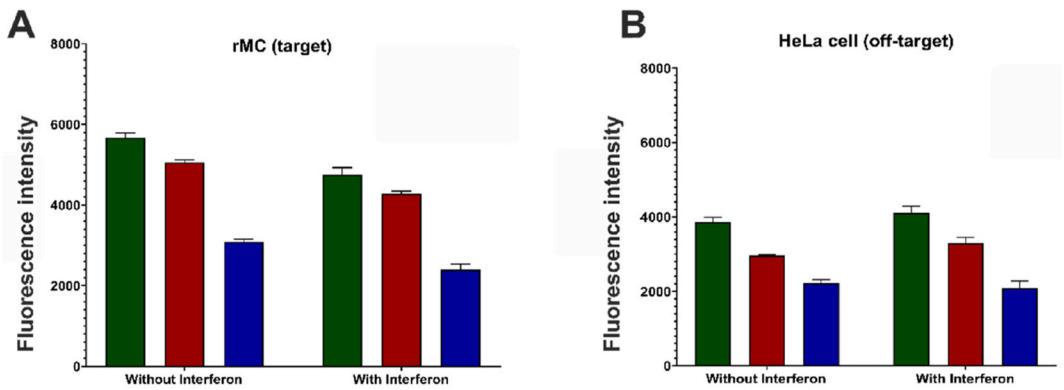

Fig. 4. Uptake of cRGD-pNP (green bar), COOH-pNP (red bar) and MeO-pNP (blue bar) into a IFN-γ pre-treated and untreated rMC (target cell)/HeLa cell (off-target cell) co-culture. The graphs represent the quantity of particle uptake by rMCs (A) or HeLa cells (B) measured as APC-A geoMean fluorescence intensity [a.u.] in the presence or absence of IFN-γ. The IFN-γ effect is significant for all polymer particles used (A). The uptake of the untreated cells are plotted on the left-hand side and the uptake of IFN-γ treated cells is plotted on the right-hand side (Fig. 4A and B). The co-culture were separated by cell line in the diagrams (Fig. 4A and B). Fig. 4A represents the uptake into the rMCs and Fig. 4B represents the corresponding uptake into the HeLa cells. Nanoparticle concentration was 2 nM, IFN-γ concentration was 100 IU and IFN-γ incubation time was 24 h, **** = P value ≤ 0.0001; *** = P value ≤ 0.001; ** = P value ≤ 0,01; * = P value ≤ 0,05; ns = P value > 0,05.

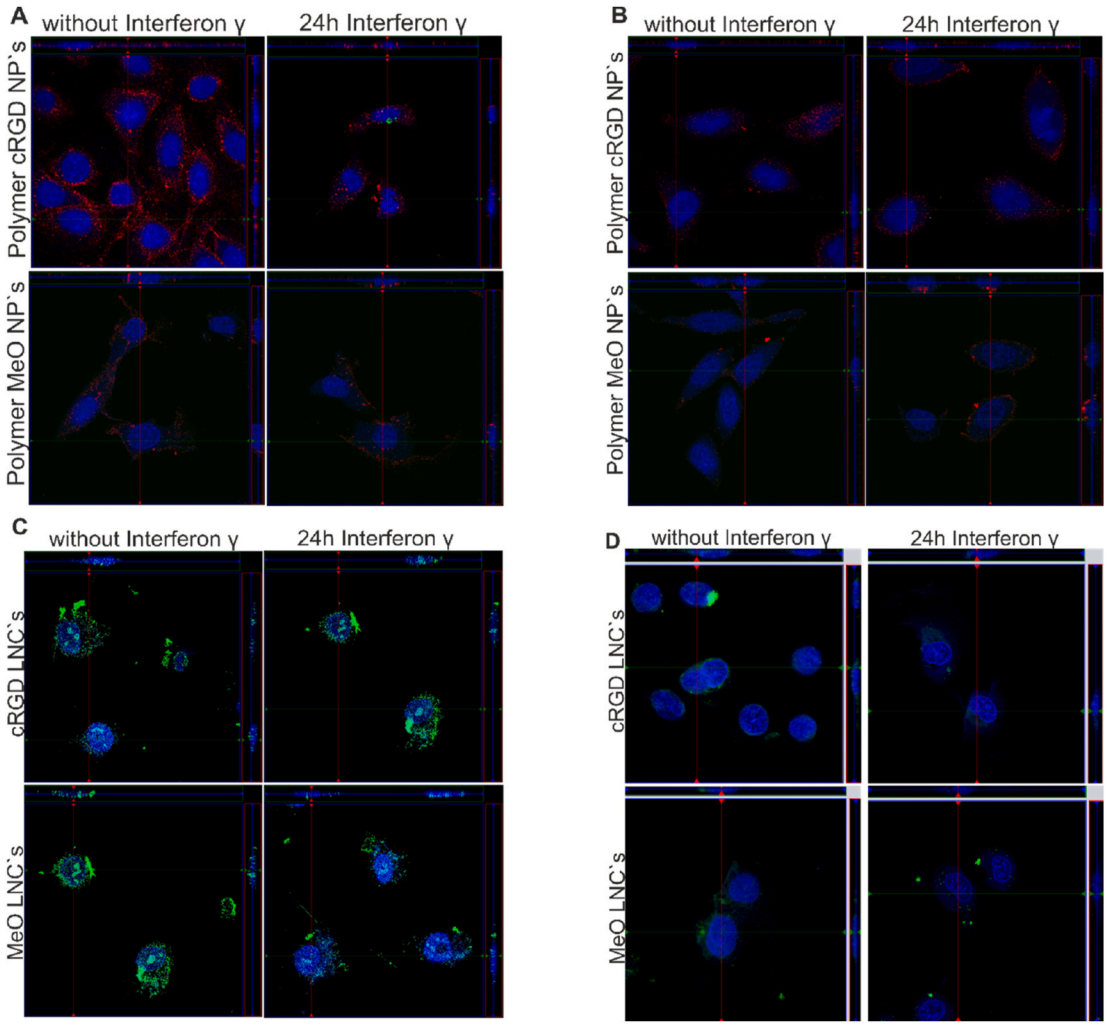

Fig. 5. Confocal microscopic images of the localization of the particles used in or on the respective cell line. The confocal microscopic images represent rMCs (A and D), HeLa cells (B) and HDMECs (C). Cell nuclei appear in blue, pNPs are visible as red dots and LNCs appears as green dots. The red lines show the location of the vertical Z-stack, and the green lines in each frame show the position of the horizontal Z-stack. Nanoparticle concentration was 0.5 nM, IFN-γ concentration was 100 IU and IFN-γ incubation time was 24 h.

However, the method cannot differentiate between particles which have crossed the cell membrane and those, which merely adhered to it. To distinguish those two modes of particle-cell interaction, confocal microscopy was used. The confocal microscopic images show rMCs (Fig. 5A/D), HeLa cells (Fig. 5B) and HDMECs (Fig. 5C) as they interact with cells. In the vertical and horizontal Z-stack, it is noticeable that the nanoparticles are distributed mostly homogeneously around the cell nucleus. Only a small number of nanoparticles forms a distinct boundary, which indicates adsorption on the cell membrane (Fig. 5). That means that only a minor fraction of the nanoparticles adheres to the cell membrane and that the nanoparticles are rather endocytosed by cells. In general, the findings of the confocal microscopy investigations confirm the results of the flow cytometry experiments. The images indicate that the target cells (rMCs) show the highest uptake of cRGD-pNP in the absence of IFN-γ (Fig. 5A). After the IFN-γ treatment, the total nanoparticle uptake decreases. There is only a slight difference in uptake of MeO-pNP into IFN-γ pre-treated and untreated rMCs (Fig. 5A). Due to the minute differences in uptake, visual differences between untreated and IFN-γ pre-treated cells are not recognizable (Fig. 5 B/C/D).

2.7. Modulation of the IFN-γ effect by the IFN-γ concentration and incubation time

First we analyzed the impact of varying IFN-γ concentrations on pNP uptake (Fig. 6A). At a concentration of 100 IU/ml IFN-γ the reduced uptake compared to the untreated cells is significant. Surprisingly, the effect vanishes with a higher IFN-γ concentrations and the difference in uptake between untreated and treated cells is no longer significant (Fig. 6A). The quantitative nanoparticle uptake also increases with increasing concentrations of IFN-γ, until no difference to untreated cells can be detected above an IFN-γ concentration of 1000 IU/ml (Fig. 6A). The data shows that the IFN- γ concentration has a decisive impact on the IFN-γ effect and can even counteract it. Next we investigated the effect of incubation time on cell uptake (Fig. 6B). First hints of the IFN-γ effect can be observed at the 6-h mark, where a slight decrease in particle uptake is noticeable, even though it is not significant. The maximum decrease in nanoparticle uptake is measured after 24 h of IFN-γ incubation. It is the only time point in our series of measurements that shows a significant decrease in uptake as a consequence of IFN-γ treatment. Particle uptake increases again with extended IFN-γ incubation times. After 30 h, no significant difference can be measured compared to the untreated sample. When the IFN-γ incubation time is increased further, the IFN-γ effect is even reversed. Thus, after 48 h of incubation with IFN-γ, we were able to measure a significant increase in particle uptake compared to untreated cells. In summary, like the IFN-γ concentration, the IFN-γ incubation time also has a major influence on the effect strength and even on the ‚direction' of the IFN-γ effect. A clear maximum effect of IFN-γ exists both in the time and the concentration domain.

2.8. Impact of 25-hydroxycholesterol (25HC) on nanoparticle uptake quantity into rMCs

As the 25 HC concentration of cell membrane is increased due to an IFN-γ treatment we investigated if it had an effect on cRGD-pNP uptake into rMCs. When cells were supplemented with 25 HC the uptake of cRGD-pNP dropped significantly (Fig. 7). The outcome demonstrates that 25 HC could play a decisive role in the mechanism of the IFN-γ effect.

3. Discussion

We found that IFN-γ causes a reduction of cRGD-decorated

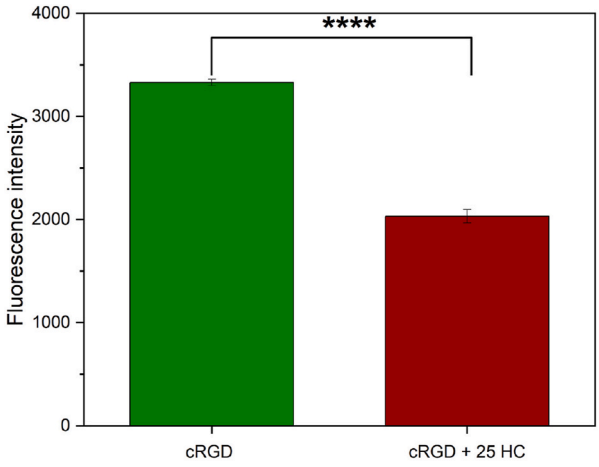

Fig. 7. Effect of 25HC on the uptake of cRGD functionalized polymer nanoparticles into untreated (green bar) and 25-hydroxycholesterol (25HC) pre-treated (red bar) rMCs. Ordinate (APC-A geoMean fluorescence intensity [a.u.]): quantity of endocytosed nanoparticles; Abscissa (treatment). Nanoparticle concentration was 2 nM, IFN-γ concentration was 100 IU and IFN-γ incubation time was 24 h. The green bar represents the uptake quantity of cRGD-pNP into rMC in untreated cells, the red bar into 25HC pre-treated cells. **** = P value ≤ 0.0001; *** = P value ≤ 0.001; ** = P value ≤ 0,01; * = P value ≤ 0,05; ns = P value > 0,05.

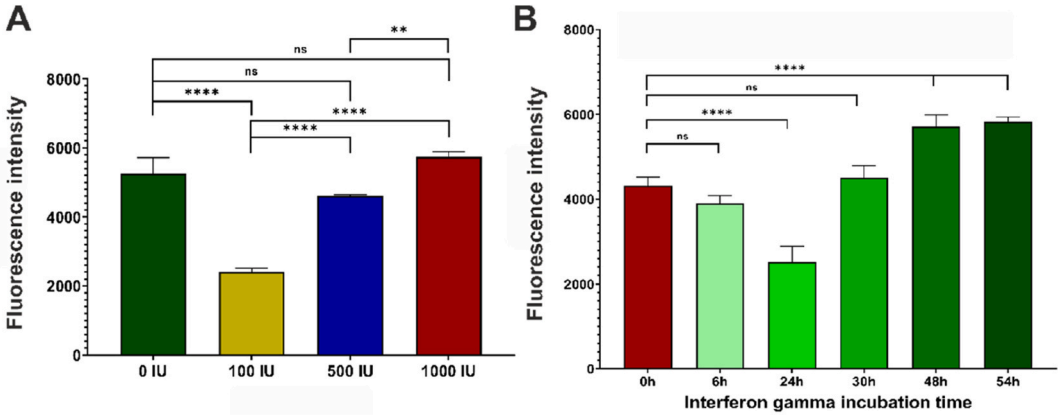

Fig. 6. Influence of the interferon gamma concentration and the interferon gamma incubation time on the IFN-γ-effect. Ordinate (APC-A geoMean fluorescence intensity [a.u.]): quantity of endocytosed nanoparticles; Abscissa (treatment). The diagrams show the uptake of cRGD polymer particles according to the IFN-γ concentration A) and the IFN-γ incubation time respoectively B). For Fig. A the incubation time in each case was 24 h. For Fig. B the IFN-γ concentration was 100 IU/ml. **** = P value ≤ 0.0001; *** = P value ≤ 0.001; ** = P value ≤ 0,01; * = P value ≤ 0,05; ns = P value > 0,05.

nanoparticle endocytosis by rMC target cells. Furthermore, in co-cultures of target with off-target cells, we observed a reduction of nanoparticle tropism, defined as the capacity of functionalized nanoparticles to differentiate between target- and off-target cell, in response to pre-incubation with IFN-γ. The results indicate that the "cellular parameters" IFN-γ concentration and IFN-γ incubation time have a pronounced effect on nanoparticle uptake, whereas the "particulate parameters" nanoparticle type and targeting ligand have only a minor influence on the IFN-γ effect.

IFN-γ effects previously ascribed to cholesterol depletion [20] must be revised, since additionally experiments in which we depleted cholesterol out of the cell membrane lead to an increased nanoparticle uptake (data not shown). Our findings suggest, that the observed IFN-γ effect could be attributed to the pronounced influence of 25-hydroxycholesterol (25HC) on membrane properties. Prior literature as well as our investigation [20] shows that IFN-γ promotes the oxidation of cholesterol to 25HC in the cell membrane via activation of cholesterol 25-hydroxylase (CH25H). Experiments that increased the 25HC content of cell membranes (Fig. 7), led to a significant reduction in nanoparticle uptake. The diminution of nanoparticular uptake by 25HC is substantial and comparable to the reduction of the nanoparticle uptake following an IFN-γ pre-treatment. Literature points at two additional pathways by which 25HC could diminish nanoparticle uptake into target cells. First, 25CH prevents the fusion of viral nanoparticles with the target cell [26–29]. This can be attributed to altered membrane properties and could apply to nanoparticles as well. Second, 25HC was found to reduce the affinity of peptide ligands and the cell membrane [33]. Due to the virus-mimetic nature of our peptide coated nanoparticles, the effect of IFN-γ could also base on this mechanism. In summary our experiments strongly suggest that the antiviral and uptake-reducing effects of HC25 described in the literature for viruses [26,28–31] is of high relevance for nanoparticle systems. IFN-γ triggers a variety of other mechanisms and effects on cells, which could contribute to the IFN-γ effect on NP uptake. For example, it is known that an IFN-γ treatment results in the arrest of cells at the G1/S checkpoint via an induction of cyclin-dependent kinase (CDK) inhibitors [32–34]. However, Kim et al. [35] reported that the influence of the cell cycle phase on nanoparticle uptake is primarily caused by cell division and is only significantly different after 28 h of continuous particle incubation. Since our experimental conditions remain far below this time frame it cannot explain the observed IFN-γ effect. We investigated also the aspect of passive uptake at 4 °C (supplementary information section). In the presence and absence of IFN-γ, the NP internalization was significantly different, but on a very low level of 5 % of the active uptake by cells at 37 °C. From this we concluded that the passive uptake has essentially no effect of the IFN-γ effects we measured.

In agreement with our tropism-transfer hypothesis the results of our study strongly suggest that the effects of IFN-γ on viruses described in literature [11–14,16–19] also apply to nanoparticles. The reduced tropism of nanoparticles caused by IFN-γ could be critical for the use of virus-mimetic nanoparticles and for nanoparticle therapy in general. As previously described, many nanoparticle therapy concepts are about targeting specific tumors. Since some tumors exhibit increased IFN-γ release compared to healthy tissue [21,22], our results suggest a central importance of our findings for tumor therapy. The benefit of functionalized nanoparticles in relation to non-functionalized nanoparticles, in particular their tendency to accumulate in target tissue, may be diminished in the presence of interferon gamma. Our results show that the effect depends on the cell type, necessitating examination of IFN-γ effects on target cells for nanoparticle therapies. Further findings that the IFN-γ effect can be minimized after a long IFN-γ incubation period or at a high IFN-γ concentration might be utilized in nanoparticle therapy as well. It is conceivable to achieve increased bioavailability by a better understanding of the IFN-γ effect.

The findings of our investigations are not limited to tumor therapy since all nucleated cells can react to IFN-γ [21]. Furthermore it is well known that IFN-γ is released in in the case of inflammatory diseases such as atherosclerosis, obesity and in the presence of pathogens or chemicals [36–41]. However, increased IFN-γ release is also observed under certain pharmacotherapies. For instance, cells of the respiratory tract secrete higher amounts of IFN-γ during asthma therapy with prednisolone [42]. In some cases, IFN-γ is directly administered during clinical therapy of tuberculosis and some types of cancer [43]. Furthermore the combination with IFN-α in the treatment of chronic hepatitis B [44] is investigated in clinical studies. The findings can be used to make future nanoparticle therapies more efficient and minimize side effects. However, further research is required to utilize the findings in practice.

It is well known that in addition to IFN-γ other interferons and cytokines influence virus cell interactions. Interferons such as IFN-α/β and tumor necrosis factors (TNF) have a particular influence on viral tropism [16,45–48]. Further studies could investigate the extent to which IFN-α/β, IFN-λ and TNF-α influence nanoparticle biodistribution. Interesting in this context is the current work of Scott G Tilden et al., which describes a possible reduction in off-target cell accumulation caused by IFN-λ, which is induced by the anti-viral innate immune response to virus-mimetic nanoparticles [49]. A synergistic influence of the pro-inflammatory cytokines on inflammatory tissue damage could be shown in the context of a SARS-CoV-2 infection [50]. Future research will have to clarify the extent to which this synergism applies to nanoparticle systems.

4. Conclusion

Overall, we can confirm our tropism-transfer hypothesis, that the effect of IFN-γ on viruses regarding their preferential uptake by target cells also applies to nanoparticle systems in general. It was shown that the effects apply broadly, albeit to varying intensities. Our results demonstrate that IFN-γ affects nanoparticle-cell interactions in a variety of ways. Thus, in the physiological range of IFN-γ incubation time and IFN-γ concentration, the tropism of the nanoparticles is reduced and the uptake into the target cells decreases. The strength of this effect depends on factors such as the particle concentration and the cell type to be addressed by nanoparticle therapy. The particle system itself appears to have less influence. We identified an altered 25HC content in the cell membrane caused by an IFN-γ pre-treatment as one of the main factors of the IFN-γ effect. In our view, further research on the effect of the body's own defense mechanisms against viruses on nanoparticles is highly valuable and beneficial for nanoparticle development.

5. Materials and methods

5.1. Materials

For the synthesis of the polymers, cRGD-PEG_{2k}-PLA_{10k}, CY5-$PLGA_{12K}$, MeO-PEG_{2k}-PLA_{10k}, COOH-PEG_{2k}-PLA_{10k} we use: c (RGDfK) synthesised by (Synpeptide, China), Carboxy-PEG_{2k} (JenKem Technology, United States), Methoxy-PEG_{2K} (Sigma-Aldrich, United States), $PLGA_{12K}$-COOH=Resomer® RG 502 H, Poly (D,L-lactide-co-glycolide, acid terminated, Mw 7000–17,000 (Sigma-Aldrich, United States), CY5-NH_2 (Lumiprobe, Germany), 1,8-Diazabicyclo [5.4.0]undec-7-ene (DBU), N-Hydroxysuccinimide (NHS), N-(3-Dimethylaminopropyl)-N′-ethylcarbodiimide hydrochloride (EDC), 2-(1H-Benzotriazole-1-yl)-1,1,3,3-tetramethyluronium hexafluorophosphate (HBTU), 3,6-Dimethyl-1,4-dioxane-2,5-dione, N,N-Diisopropylethylamine (DIPEA), SpectraPor®1 Dialyse Membrane-Standard RC Tubing 6–8 kD (Spectrum Laboratories, Inc., United States). The upconcentration of the nanoparticles was realised with Microsep Advance with 30k Omega 24/pk (Pall, United States). CellTracker™ Green (Invitrogen™, Thermo Fisher Scientific, United States), 4′,6-Diamidino-2-phenyl-indol -dihydrochlorid (DAPI) (Sigma-Aldrich, United States) and 3,3′-Dioctadecyloxacarbocyanine Perchlorate (DiO) (Invitrogen™, Thermo Fisher Scientific, United States) was used for staining the cells. For the

cell culture we used Endothelial Cell Growth Medium MV (PromoCell GmbH, Germany), RPMI-1640 Medium (powder, with L-glutamine, without sodium bicarbonate) (Sigma-Aldrich, United States), Minimum Essential Medium Eagle (EMEM) (with Earle's salts, L-glutamine and non-essential amino acids, without sodium bicarbonate, powder) (Sigma-Aldrich, United States), Insulin-Transferrin-Selenium 100X (ITS) (Gibco™, Thermo Fisher Scientific, United States), Fetal bovine serum (South America Origin) (FBS) (Batch number: P201004, PAN-Biotech, Germany), Trypsin 0,25 %/EDTA 0,02 % in PBS w/o Calcium and Magnesium (Trypsin) (PAN-Biotech, Germany). Further we used Dulbecco's Phosphate Buffered Saline (DPBS), Leibovitz's L-15 Medium both from (Gibco™, Thermo Fisher Scientific, United States), Endothelial Cell Basal Medium MV (prf) (PromoCell GmbH, Germany), Hydrocortisone (Sigma Aldrich, United States), Interferon γ (INF-γ), Rat (GenScript, United States). The Milli-Q® EQ (7000) device provided the millipore water. Octamethylcyclotetrasiloxane (OMS) (Sigma-Aldrich, United States) was used as a lipophilic standard for cholesterol quantification.

5.2. Methods

5.2.1. Polymer synthesis

The syntheses of the polymers have already been published [7,51] therefore the procedures will only be described in brief:

5.2.2. Synthesis of COOH-PEG$_{2K}$-PLA$_{10K}$

In the initial step, 3 g 3,6-dimethyl-1,4-dioxane-2,5-dione was purified from possible residual water by recrystallisation in 6 ml ethyl acetate (85 °C) and dried for 12 h under vacuum. 348 mg (mol) COOH-PEG$_{2K}$-OH was dried under vacuum for 12 h at 40 °C while stirring the melt in a round bottom flask with a magnetic stirrer. The dried COOH-PEG$_{2K}$-OH was dissolved in 10 mL of anhydrous DCM. 1666 mg 3,6-dimethyl-1,4-dioxane-2,5-dione and 573 µl 1,8-diazabicyclo [5.4.0] undec-7-ene were added to the solution. The reaction mixture was stirred in a round bottom flask for exactly 1 h before quenching with 351 mg benzoic acid. The mixture was precipitated in 200 ml ice-cold diethyl ether. The copolymer was dissolved in 1 ml acetonitrile and then precipitated again in 200 ml ice-cold diethyl ether. The dissolution and precipitation step were repeated one more time before the copolymer was dried under vacuum for 12 h at 40 °C–45 °C.

5.2.3. Synthesis of MeO-PEG$_{2K}$-PLA$_{10K}$

The synthesis of MeO-PEG$_{2K}$-PLA$_{10K}$ was performed as COOH-PEG$_{2K}$-PLA$_{10K}$ synthesis, with the difference that 325 mg MeO-PEG$_{2K}$-OH was used instead of 348 mg COOH-PEG$_{2K}$-OH.

5.2.4. Synthesis of cRGD-PEG$_{2K}$-PLA$_{10K}$

99 mg of 1-Ethyl-3-(3-dimethylaminopropyl)carbodiimide (EDC), 60 mg of N-Hydroxysuccinimide (NHS) and 310 mg of PLA10k-PEG2k-COOH were added to a glass vial, dissolved in 1 mL anhydrous DMF and stirred for 3 h at room temperature. To quench the reaction, 72 µl of 2-mercaptoethanol was added to the mixture and stirred at room temperature for further 15 min 19 mg cRGDfK, dissolved in 500 µl anhydrous N,N-Dimethylformamide 99.8 % (DMF) and 54 µl N,N-diisopropylethylamine (DIPEA) was added and stirred for 48 h at room temperature. The product was dialyzed against millipore water using a dialysis membrane standard RC Tubing 6–8 kD for 24 h. Millipore water was exchanged after 0.5, 1, 2, 4 and 6 h. The solution was lyophilized for 5 days.

5.2.5. 9,10-Phenanthrenequinone assay (PCA-assay)

The PCA-assay was performed to quantify the coupling efficiency of cRGDfK to the polymer. 10 mg cRGDfK were dissolved in 10 mL millipore water (stock solution). 300 µL of a cRGD-PEG$_{2K}$-PLA$_{10K}$ solution in acetonitrile at a concentration of 10 mg/mL was dropped into 2.7 mL of Millipore water and stirred (800 rpm) at room temperature for 3 h (Sample solution). 300 µL PLA$_{10k}$-PEG$_{2k}$-COOH with a concentration of 10 mg/ml in acetonitrile was added dropwise into vigorously stirring (800 rpm) solution of 0.14 mL of cRGDfK stock solution and 2.56 mL of Millipore water. The solution was stirred at room temperature for 3 h (Standard solution). The standard solution had a concentration of cRGD referring to 100 % coupling efficiency of cRGDyK-PEG2k-PLA10k synthesis. For recording a calibration curve 250 µL of this standard solution were pipetted into Eppendorf tubes and diluted with Millipore water to obtain dilutions referring to 100 %, 75 %, 50 %, 25 % and 0 % coupling efficiency. 250 µL of each dilution and sample were pipetted in triplicates into Eppendorf tubes. The final working solutions were obtained adding 125 µL of a mixture of 6 parts of a 9,10-phenanthrene quinone solution (150 µM in ethanol) with one part of 2N NaOH. 875 µL of working solution were added to each of the prepared Eppendorf tubes and incubation at 60 °C for 3 h. An aliquot of 125 µl was taken from each Eppendorf tube and mixed with 125 µl of a 1N HCl. The samples were transferred into black 96 well plate and stirred with an orbital shaker at room temperature for 1 h at 125 rcf. The fluorescence was measured by exciting at 312 nm and measuring the emission at 395 nm. To create the calibration curve, the emission was plotted against the coupling efficiency in %. The coupling efficiency was determined from the emission of the sample. The PCA-assay for the LNC nanoparticles was performed after preparation and functionalization in the same way as for the polymer nanoparticles. The evaluation of the PCA-assay was attached to the supplementary information section.

5.3. Polymer characterization

5.3.1. Synthesis of CY5-PLGA

1 mg CY-5-NH2, 184 mg Resomer® RG 502 H, Poly (D,L-lactide-co-glycolide, acid terminated, Mw 7000–17,000 (PLGA$_{12K}$-COOH) and 12 mg O-(Benzotriazol-1-yl)-N,N,N′,N'-tetramethyluronium-hexafluorophosphat (HBTU) were dissolved in as little DMF as possible. 11 µL N,N-Diisopropylethylamin (DIPEA) was added and the mixture was stored in the refrigerator overnight at −20 °C, protected from light. The mixture was added dropwise into 45 ml of ice-cold diethyl ether and the precipitate spun down by centrifugation at 3000 rpm. The supernatant diethyl ether was decanted, and the precipitate was dried in a nitrogen stream. The dry product was dissolved in 5 mL acetonitrile and precipitated again in ice-cold diethyl ether. The process was repeated until the diethyl ether supernatant is no longer blue, but at least 3 times. The product was dried in under vacuum at room temperature for 24 h.

5.3.1.1. Polymer nanoparticle preparation. The polymer nanoparticles were produced by dropwise addition of polymer solution into vigorously stirring solution of 10 % PBS. The composition of the polymer solution for each nanoparticle is shown in Table 1. The concentration of the stock solution of each component was 10 mg/ml (in acetonitrile).

The solution was stirred for 3 h at 800 rpm. The particles were ultracentrifuged (Microsep®Advance centrifugation filter 30k) at 3000 rcf for 30 min 1 ml of Leibovitz's L-15 medium was added to the concentrated particles. The particles were measured using nanoparticle tracking analysis and adjusted to the respective concentration with Leibovitz's L-15 medium.

5.3.1.2. Lipid nanocapsules (LNCs) preparation. The LNC preparation and functionalization has already previously been published [52]. In short: approximately 4000 mg of Kolliphor® HS 15 was weighed into a Falcon tube and mixed with Millipore water to produce a 40 % (m/m)

Table 1

Particle	CY5-PLGA [µl]	PLA$_{10k}$-PEG2$_k$-MeO [µl]	PLA$_{10k}$-PEG$_{2k}$-cRGD [µl]
cRGD-NP	90	X	210
MeO-NP	90	210	X

solution. To obtain a clear solution, the mixture was heated briefly to 50 °C. 887 mg of the resulting Kolliphor® HS 15 solution, 30 mg 1,2-dioleoyl-sn-glycero-3-phosphocholine (DOPC), 415 mg Miglyol 812, 12 mg of a 1 % NaCl solution (m/m) in Millipore water, 656 mg Millipore water and 2 mg 3,3′-Dioctadecyloxacarbocyanine Perchlorate (DiO) were weighed into a glass vial with plastic lid. The mixture was heated to 90 °C under stirring at 300 rpm. Next, the solution was cooled down to 60 °C. This process of heating and cooling was repeated two more times. The stirring speed was increased to 700 rpm during the last cooling cycle and 5 mL Millipore water were added at a temperature of 78 °C (the solution must still be clear). After addition of water, the mixture was stirred for another 5 min. The spontaneously forming LNCs were filtered with a 0.2 μm RC syringe filter and stored protected from light at room temperature. The LNCs were characterized using nanoparticle tracking analysis.

5.4. Functionalization of lipid nanocapsules (LNCs)

A cRGDfC stock solution was prepared in Millipore water with a concentration of 1 mg/mL. DSPE-PEG_{2k}-Mal and DSPE-mPEG_{2k} were each dissolved in DPBS to obtain a stock solution with a concentration of 12 mg/mL 80 μL cRGDfC stock solution, 201 μL DPBS and 16.94 μL DSPE-PEG_{2k}-Mal stock solution were pipetted into an Eppendorf tube (Tube 1). 281 μ L DPBS and 16.16 μL of the DSPE-mPEG_{2k} stock solution to were added in another Eppendorf tube (Tube 2). Tube 1 and 2 were shaken under exclusion of light for 2 h at room temperature. 21.5 μL of LNC solution was added to both tubes before shaking the samples for further 3 h at 37 °C under light exclusion. The samples were cooled for 5 min in water with a temperature below 5 °C. For the purification of the functionalized LNC solutions, the samples were each placed in a Microsep®Advance centrifugation filter 30k, diluted with 4 ml DPBS and centrifuged at 1500 g for 15 min. The filters were refilled with 4 ml DPBS and centrifuged again with the same settings. The functionalized LNCs were measured using nanoparticle tracking analysis.

5.5. Nanoparticle tracking analysis (NTA)

We characterized the hydrodynamic diameter and the size distribution of polymer nanoparticles and LNCs via nanoparticle tracking analysis (NTA) using a NanoSight NS300 (Malvern Panalytical, United Kingdom). For a measurement, we diluted the respective nanoparticle sample 1:10000 with Millipore water. The samples were injected into the system with a syringe and a flow cell was used for the measurement. We measured with the following capture settings: screen gain: 2; camera level: 16; number of captures: 3 (N = 3) and with a capture duration of 60 s. The settings for the process were set to a screen gain of 10 and a detection threshold of 3. The Polydispersity Index (PDI) can be calculated from the measurement data by squaring the quotient of the standard deviation and the mean of the hydrodynamic diameter. (The results of the NTA measurements are attached to the supplementary information section).

5.6. Characterization of PLA_{10k}-PEG_{2k} block copolymers with ^1H NMR

^{1}H NMR spectra were taken on a Bruker Avance-400 or Avance-500 NMR spectrometer (Bruker). 20 mg of each sample were dissolved in 700 μL $CDCl_3$ (Chloroform-d) and transferred to a NMR Tube (Deutero GmbH) for the measurement. By integrating signals with the TopSpin software 4.0.8 (Bruker Corporation, Billerica, MA, USA), the numerical average molecular weight of the PLA_{10k}-PEG_{2k} block copolymers was calculated. The number of oxyethylene units in the PEG chain was calculated by dividing the molecular mass specified by the manufacturer, by the molecular mass of the repeating units (44.03 g/mol). Since oxyethylene contains four protons (–OC$\mathbf{H_2}$C$\mathbf{H_2}$–) a 2 kDa PEG (PEG_{2k}) chain contains 182 protons. The ratio of the polyethylene glycol (PEG) signal integral divided by 182 served as a calibration to calculate the number of monomers in the polylactic acid (PLA) chain of the block-copolymer. To this end the integral of the PLA signal was determined and calculated as number of protons. PLA shows two relevant peaks in an ^{1}H NMR spectrum. The first peak (–CH_3) was located at about 1.6 ppm and the second peak (–CH–) at 5.2 ppm. The number of monomers in the PLA chain was calculated as the sum of the signal integrals ($A_{PLA\ CH3}$ and $A_{PLA\ CH}$) divided by the respective number of protons (Equation (1)).

$$\text{Number of PLA units} = \frac{A_{PLA\ CH_3}}{3} + \frac{A_{PLA\ CH}}{1} \qquad \text{(Equation 1)}$$

The entire molecular mass of the PLA_{10k}-PEG_{2k} block copolymer was calculated by multiplying the mean number of PLA units by the molecular weight of a single PLA repeating unit (72.06 g/mol), which yields the molecular mass of the PLA chain. To this was added the molecular weight of the PEG chain. Represented in equation (2) below.

$$M(PLA-PEG) = \frac{\frac{A_{PLA\ CH_3}}{3} + \frac{A_{PLA\ CH}}{1}}{2} \cdot 72.06\ \frac{g}{mol} + M(PEG) \qquad \text{(Equation 2)}$$

The ^{1}H NMR spectra of the MeO- and COOH- PLA_{10k}-PEG_{2k} block copolymers are attached to the supplementary information section.

5.7. Cell culture

5.7.1. General information

Rat mesangial cells (rMC) were cultivated on RPMI-1640 Medium supplemented with 10 % (v/v) FBS, 1 % (v/v) ITS and 100 μM hydrocortisone (rMC-medium). We used Minimum Essential Medium Eagle (EMEM) for the HeLa cells and Endothelial Cell Growth Medium MV for the HDMECs. For all experiments, we used always rMCs in the 78th passage/HDMECs in the 5th passage and HeLa cells between the 40th and 50th passage. The cells were always 80 %–90 % confluent (T75 flask) at the time of the experiment/preparation for the experiment. Interferon was supplemented 24 h after cell seeding.

5.7.2. Detachment of the cells

First, the cells were washed with pre-warmed DPBS and then detached from the bottom of the cell culture plate with trypsin (5 min, 37 °C, 5 % CO2). The cell suspension was mixed with twice the amount of the respective cell medium to neutralize the trypsin that had previously been added. The suspension was then transferred to a falcon tube and centrifuged at 200 rcf for 5 min. The supernatant was aspirated, and the cells were resuspended in the respective cell medium.

5.7.3. Cell staining for flow cytometry

In the case of co-culture experiments, it was necessary to stain a cell species to be able to distinguish the cells in the flow cytometry. Therefore, we stained the rMCs with CellTracker Green (CTG). To this end 50 μg CTG were dissolved in 11 μL anhydrous DMSO. The solution was pipetted into 10989 μl rMC-Medium without FBS (staining solution). The rMCs were detached as described and resuspended in the staining solution after aspiration of the supernatant. The cell suspension was pipetted into a Petri dish, covered with aluminium foil, and stirred for 50 min at 37 °C and 5 % CO_2 (50 rpm). Subsequently, the cell suspension was transferred to a Falcon tube and centrifuged at 200 rcf for 5 min. The supernatant was removed, and the cells were resuspended in DPBS. The cells were centrifuged again at the same settings and the supernatant was aspirated again. The rMCs were resuspended in rMC medium.

5.7.4. Cell staining for confocal microscopy

For confocal microscopy, cell nuclei were stained with DAPI and the cell membrane respectively the lipophilic intracellular structures with DiO. For this, a DiO stock solution was prepared by dissolving 1.76 mg DiO in 0.5 mL DMSO and adding the same volume of ethanol. For a better solubilization of DiO, the mixture was heated to 55 °C. 2.5 μl of the DiO stock solution was diluted with 997.5 μL of DPBS to prepare the

final DiO solution for staining. For staining the cell nuclei, 10 μL DAPI were mixed with 990 μL DPBS. The cells were fixed with 250 μL of 4 % paraformaldehyde solution for 10 min before staining. After fixation, the cells were washed 3 times with DPBS (250 μL) and then incubated with 250 μL DiO solution for 15 min at room temperature in the absence of light. Before nuclei staining, the cells were washed again 3 times and then incubated with 250 μL DAPI solution for 10 min in the absence of light at room temperature. After DAPI staining, the cells were washed again 3 times and stored over DPBS in the dark at 4 °C.

5.7.5. Cell counting

For the cell counting and setting the number of cells of the respective experiments, we used a Neubauer improved cell counting chamber (Paul Marienfeld, Germany).

5.7.6. Interferon treatment

The 100 IU/ml interferon gamma working solution was prepared by adding 1.1 μL interferon stock solution ($1.0*10^6$ IU interferon gamma in 1 ml DPBS) to 11 mL of the respective cell medium. The 500 IU/ml and 1000 IU/ml interferon gamma working solutions were prepared by adding 5.5 μL and 11 μL respectively of the interferon stock solution to 11 mL of the respective cell medium. After a 24-h growth period, the medium above the cells was aspirated and replaced with 500 μL per well of the respective interferon-containing cell medium. In the case of the control group, the medium was also aspirated but replaced with the respective interferon-free cell medium. This was done to exclude a possible alteration of the results by changing the medium. The interferon incubation time varied between the trials.

5.7.7. Enhancement of the 25-hydroxycholesterol (25HC) content of the cell membrane

Enhancement of the 25-hydroxycholesterol (25HC) content in the cell membrane was done in analogy to increasing the cholesterol content in the cell membrane, which was extensively published [53]. Therefore, only a brief mention will be made:

25 mg of 25HC were weighed in a glass vial and dissolved in 1 mL of a chloroform/methanol (1:1 v:v) solution. 100 μL of this 25HC solution were heated in a glass vial to 80 °C to evaporate the solvents. Methyl-β-Cyclodextrin (MβCD) was dissolved in serum free RPMI medium to obtain a 5 mM MβCD solution. 5.18 mL of the MβCD solution were added to the 25HC solid. To dissolve the 25HC, the mixture was sonicated for 10 min in cycles of 8 s with 4 s of switched-on ultrasonic bath and 4 s of switched-off ultrasonic bath. The clear 25HC/MβCD solution was vortexed intensely for 5 min. The preparation was warmed up to 37 °C in a water bath, before 300 μL of the solution was added for 30 min to each well of a 24 well plate to enrich the cell membrane with 25HC.

5.8. Flowcytometry

Flow cytometry was used to quantify nanoparticle uptake into cells. To distinguish in the co-culture between the rMCs and the HeLa cells in the flow cytometry, we stained the rMCs with CellTracker Green. We coupled Cy5, a red fluorescence dye, to the PLGA block of our polymeric nanoparticles and we stained the LNCs with DiO, a lipophilic fluorescent dye to be capable to measure the uptake ratio of our nanoparticle by the flow cytometry. For analysis the BD FACSCanto™ II and the BD LSRFortessa™ cell analyzer (both BD Biosciences, United States) were used. Samples were always measured in triplicate (n = 3) using the parameters shown in Tables 2 and 3 for LNCs and polymer nanoparticles respectively.

Cells were seeded into 24- or 96 well plates at 80 %–90 % confluency. INF-γ was added to the cells at the earliest 24 h after seeding to ensure attachment of all cell lines used. Before the particle solution was added to the cells, they were washed 3 times with 300 μl DPBS per well. Each well was then incubated with 300 μl of pre-warmed (37 °C) particulate solution for 75 min (polymer nanoparticle concentration: 0.1 nM and LNC concentration: 1 nM). After incubation, the solution of particles was removed, and each well was washed 3 times with 300 μL of pre-warmed DPBS (37 °C). To detach the cells, 200 μL of trypsin 0.25 % was pipetted into each well after aspiration of the supernatant. The plates were then kept for 5 min in the incubator (37 °C, 5 % CO_2). Complete detachment of the cells was verified using a light microscope. 500 μL of cell medium was pipetted into each well of the cell-trypsin suspension. In the case of using tubes for measurement, the cell suspension was transferred into a 2 mL Eppendorf tube (each well into an Eppendorf tube) and centrifuged (200 rcf, 5 min, 4 °C). The supernatant was aspirated, and the cells were resuspended with cold DPBS (4 °C) in the Eppendorf tube and centrifuged with the same settings. The supernatant was removed again, and the cells were resuspended once more in 300 μL cold DPBS. Prior to the measurement, the cell suspension was then pipetted into a 5 mL tube (75 * 12 mm, PS) (Sarstedt, Germany). In the case of using a BD High Throughput Sampler (HTS) (BD Biosciences, United States), 200 μL of the cell suspension was pipetted into a 96 well plate. The cell suspension from one well of a 24 well plate was transferred to 3 wells of the 96 well plate. The 96 well plate was measured using the HTS unit. Depending on the investigated nanoparticles, the voltages of the detectors used are specified in the subsequent table.

5.9. Confocal microscopy

The information about the location of the nanoparticles in cells was obtained by confocal microscopy. cRGD-/MeO-polymer nanoparticles and cRGD-/Meo-LNCs were used for confocal microscopy. Cells were incubated with polymer nanoparticles at a concentration of 0.75 nM and lipid nanocapsules of 1 nM respectively. Polymer nanoparticles were stained with CY5 to make them visible, LNCs were stained with DiO. To achieve 80 %–90 % confluency, 1250 rMCs, 6500 HeLa cells and 10000 HDMECs were seeded per well (μ-Slide 8 Well ibiTreat) (Ibidi GmbH, Germany). Optionally, cells were IFN-γ treated 24 or 48 h before cell fixation (see cell staining for Confocal microscopy). Z-stack images were taken to identify whether the particles were taken up by the cells or attached to their surface. Zeiss LSM 710 (Carl Zeiss AG, Germany) was used for our investigations.

5.9.1. Cell viability determined by MTT assay

The use of the 3-(4,5-Dimethylthiazol-2-yl)-2,5-diphenyltetrazoliumbromid (MTT) assay is a widely used method for determining cell viability [54–56]. In brief: In a 96 well plate, 2500 cells were seeded in 100 μL RPMI (+10 % FBS, +HC, +ITS) medium per well. The outer, peripheral wells were filled with PBS for evaporation protection. After 24 h of incubation, the supernatant was aspirated. 100 μL of the respective nanoparticle dispersion or medium (with or without IFN-γ)

Table 2
Parameters used for the determination of LNC uptake via FACS.

Parameter	Voltage
Forward scatter (FCS)	0
Sideward scatter (SSC)	150
FITC detector setting	370
APC detector setting	350

Table 3
Parameters used for the determination of polymer nanoparticle uptake via FACS.

Parameter	Voltage
FCS	0
SSC	150
FITC detector setting	250
APC detector setting	350

were pipetted into the wells (n = 6). Untreated cells were used as "100 % control" and 0,1 % SDS in RPMI medium treated cells were used as positive control. The cells were incubated for further 24 h 3.75 mL MTT stock solution (19.36 mg MTT dissolved in 7.74 mL PBS and sterile filtered) was mixed with 10.9 mL RPMI medium and 0,4125 mL FCS to obtain the MTT working solution (0.625 mg/mL MTT as final concentration). The cell distribution and cell morphology were assessed by microscopy. After aspiration of the medium, 200 µL MTT working solution was added to the cells and incubated for 3 h at 37 °C. The supernatant was then carefully aspirated and 100 µl of a 10 % SDS in PBS solution was added to the cells. The plates were sealed tightly with Parafilm and incubated overnight in the absence of light. The plates were then gently moved and measured at 570 nm and 690 nm (absorption and transmission). For further information see supplementary information section.

5.10. Data analysis

The raw flow cytometry data acquired with BD FACSCanto™II and BD LSRFortessa™ cell analyzer (both BD Biosciences, United States) was analyzed with the Flowing Software (v2.5.1, Cell Imaging and Cytometry Core, Turku Bioscience Centre, Turku, Finland, with the support of Biocenter Finland).

The data from the confocal microscope was edited and processed using the ZEN blue software (Version 3.6.095.01000, Carl Zeiss Microscopy GmbH, Germany).

5.11. Statistical evaluation

Depending on the experimental design, a one-way ANOVA or two-way ANOVA was conducted via GraphPad Prism 8.0.1 software. The alpha level was defined as 0.05 for each statistical evaluation. The P value was determined as follows: **** = P value ≤ 0.0001; *** = P value ≤ 0.001; ** = P value ≤ 0,01; * = P value ≤ 0,05; ns = P value > 0,05.

CRediT authorship contribution statement

Marius Remmert: Writing – original draft, Visualization, Validation, Resources, Methodology, Investigation, Formal analysis, Data curation, Conceptualization. **Johannes Konrad:** Writing – review & editing, Methodology. **Jan Birringer:** Writing – review & editing, Methodology. **Achim Goepferich:** Writing – review & editing, Writing – original draft, Supervision, Project administration, Methodology, Funding acquisition, Conceptualization.

Declaration of competing interest

The authors declare that they have no known competing financial interests or personal relationships that could have appeared to influence the work reported in this paper.

Acknowledgments

This work was supported by German Research Foundation (Deutsche Forschungsgemeinschaft, DFG), grant GO 565/20-1.

The authors thank Prof. Miriam Breunig for her assistance and the manifold productive dialogues about the performed investigations. The authors would particularly like to thank Renate Liebl for her outstanding technical expertise.

Appendix A. Supplementary data

Supplementary data to this article can be found online at https://doi.org/10.1016/j.jddst.2025.107301.

Data availability

Data will be made available on request.

References

[1] V. Cagno, SARS-CoV-2 cellular tropism, Lancet Microbe 1 (2020) e2–e3, https://doi.org/10.1016/S2666-5247(20)30008-2.
[2] U. AbuBakar, L. Amrani, F.A. Kamarulzaman, S.A. Karsani, P. Hassandarvish, J. E. Khairat, Avian influenza virus tropism in humans, Viruses 15 (2023), https://doi.org/10.3390/v15040833.
[3] C.J.A. Duncan, Q.J. Sattentau, Viral determinants of HIV-1 macrophage tropism, Viruses 3 (2011) 2255–2279, https://doi.org/10.3390/v3112255.
[4] K. Watashi, T. Wakita, Hepatitis B virus and hepatitis D virus entry, species specificity, and tissue tropism, Cold Spring Harb. Perspect. Med. 5 (2015) a021378, https://doi.org/10.1101/cshperspect.a021378.
[5] E.S. Lee, D. Kim, Y.S. Youn, K.T. Oh, Y.H. Bae, A virus-mimetic nanogel vehicle, Angew Chem. Int. Ed. Engl. 47 (2008) 2418–2421, https://doi.org/10.1002/anie.200704121.
[6] S. Maslanka Figueroa, D. Fleischmann, A. Goepferich, Biomedical nanoparticle design: what we can learn from viruses, J. Contr. Release 329 (2021) 552–569, https://doi.org/10.1016/j.jconrel.2020.09.045.
[7] S. Maslanka Figueroa, A. Veser, K. Abstiens, D. Fleischmann, S. Beck, A. Goepferich, Influenza A virus mimetic nanoparticles trigger selective cell uptake, Proc. Natl. Acad. Sci. U. S. A 116 (2019) 9831–9836, https://doi.org/10.1073/pnas.1902563116.
[8] A. Roldão, M.C.M. Mellado, L.R. Castilho, M.J.T. Carrondo, P.M. Alves, Virus-like particles in vaccine development, Expert Rev. Vaccines 9 (2010) 1149–1176, https://doi.org/10.1586/erv.10.115.
[9] L. Wang, X. Wang, F. Yang, Y. Liu, L. Meng, Y. Pang, M. Zhang, F. Chen, C. Pan, S. Lin, X. Zhu, K.W. Leong, J. Liu, Systemic antiviral immunization by virus-mimicking nanoparticles-decorated erythrocytes, Nano Today 40 (2021) 101280, https://doi.org/10.1016/j.nantod.2021.101280.
[10] S. Wilhelm, A.J. Tavares, Q. Dai, S. Ohta, J. Audet, H.F. Dvorak, W.C.W. Chan, Analysis of nanoparticle delivery to tumours, Nat. Rev. Mater. 1 (2016), https://doi.org/10.1038/natrevmats.2016.14.
[11] G.K. Binder, D.E. Griffin, Interferon-gamma-mediated site-specific clearance of alphavirus from CNS neurons, Science 293 (2001) 303–306, https://doi.org/10.1126/science.1059742.
[12] M. Blanc, W.Y. Hsieh, K.A. Robertson, K.A. Kropp, T. Forster, G. Shui, P. Lacaze, S. Watterson, S.J. Griffiths, N.J. Spann, A. Meljon, S. Talbot, K. Krishnan, D. F. Covey, M.R. Wenk, M. Craigon, Z. Ruzsics, J. Haas, A. Angulo, W.J. Griffiths, C. K. Glass, Y. Wang, P. Ghazal, The transcription factor STAT-1 couples macrophage synthesis of 25-hydroxycholesterol to the interferon antiviral response, Immunity 38 (2013) 106–118, https://doi.org/10.1016/j.immuni.2012.11.004.
[13] R. Burdeinick-Kerr, D. Govindarajan, D.E. Griffin, Noncytolytic clearance of sindbis virus infection from neurons by gamma interferon is dependent on Jak/STAT signaling, J. Virol. 83 (2009) 3429–3435, https://doi.org/10.1128/JVI.02381-08.
[14] T.M. Kündig, H. Hengartner, R.M. Zinkernagel, T cell-dependent IFN-gamma exerts an antiviral effect in the central nervous system but not in peripheral solid organs, J. Immunol. 150 (1993) 2316–2321.
[15] S.-Y. Liu, R. Aliyari, K. Chikere, G. Li, M.D. Marsden, J.K. Smith, O. Pernet, H. Guo, R. Nusbaum, J.A. Zack, A.N. Freiberg, L. Su, B. Lee, G. Cheng, Interferon-inducible cholesterol-25-hydroxylase broadly inhibits viral entry by production of 25-hydroxycholesterol, Immunity 38 (2013) 92–105, https://doi.org/10.1016/j.immuni.2012.11.005.
[16] G. McFadden, M.R. Mohamed, M.M. Rahman, E. Bartee, Cytokine determinants of viral tropism, Nat. Rev. Immunol. 9 (2009) 645–655, https://doi.org/10.1038/nri2623.
[17] B. Parra, D.R. Hinton, N.W. Marten, C.C. Bergmann, M.T. Lin, C.S. Yang, S. A. Stohlman, IFN-gamma is required for viral clearance from central nervous system oligodendroglia, J. Immunol. 162 (1999) 1641–1647.
[18] A. Steed, T. Buch, A. Waisman, H.W. Virgin, Gamma interferon blocks gammaherpesvirus reactivation from latency in a cell type-specific manner, J. Virol. 81 (2007) 6134–6140, https://doi.org/10.1128/jvi.00108-07.
[19] M. Trilling, V.T.K. Le, A. Zimmermann, H. Ludwig, K. Pfeffer, G. Sutter, G.L. Smith, H. Hengel, Gamma interferon-induced interferon regulatory factor 1-dependent antiviral response inhibits vaccinia virus replication in mouse but not human fibroblasts, J. Virol. 83 (2009) 3684–3695, https://doi.org/10.1128/JVI.02042-08.
[20] O. Zimmer, M. Walter, M. Remmert, O. Maier, R. Witzgall, A. Goepferich, Impact of interferon-γ on the target cell tropism of nanoparticles, J. Contr. Release 362 (2023) 325–341, https://doi.org/10.1016/j.jconrel.2023.08.034.
[21] A.M. Gocher, C.J. Workman, D.A.A. Vignali, Interferon-γ: teammate or opponent in the tumour microenvironment? Nat. Rev. Immunol. 22 (2022) 158–172, https://doi.org/10.1038/s41577-021-00566-3.
[22] D. Jorgovanovic, M. Song, L. Wang, Y. Zhang, Roles of IFN-γ in tumor progression and regression: a review, Biomark. Res. 8 (2020) 49, https://doi.org/10.1186/s40364-020-00228-x.
[23] Daniel Fleischmann, Virus-Mimetic Nanoparticles for the Therapy of Mesangial Cells in Diabetic Nephropathy, Dissertation, Regensburg, 2021.
[24] E.G. Fischer, Glomerular mesangial cell adhesion to fibrinogen is mediated by αvβ3 integrin, Biochem. Cell. Biol. 82 (2004) 597–601, https://doi.org/10.1139/o04-051.

[25] D. Fleischmann, S. Maslanka Figueroa, A. Goepferich, Steric shielding of cRGD-Functionalized nanoparticles from premature exposition to off-target endothelial cells under a physiological flow, ACS Appl. Bio Mater. 4 (2021) 640–650, https://doi.org/10.1021/acsabm.0c01193.
[26] S. Wang, W. Li, H. Hui, S.K. Tiwari, Q. Zhang, B.A. Croker, S. Rawlings, D. Smith, A.F. Carlin, T.M. Rana, Cholesterol 25-Hydroxylase inhibits SARS-CoV-2 and other coronaviruses by depleting membrane cholesterol, EMBO J. 39 (2020) e106057, https://doi.org/10.15252/embj.2020106057.
[27] P. Pereiro, G. Forn-Cuní, S. Dios, J. Coll, A. Figueras, B. Novoa, Interferon-independent antiviral activity of 25-hydroxycholesterol in a teleost fish, Antivir. Res. 145 (2017) 146–159, https://doi.org/10.1016/j.antiviral.2017.08.003.
[28] C. Nguyen, J. Saint-Pol, S. Dib, C. Pot, F. Gosselet, 25-Hydroxycholesterol in health and diseases, J. Lipid Res. 65 (2024) 100486, https://doi.org/10.1016/j.jlr.2023.100486.
[29] B. Gomes, S. Gonçalves, A. Disalvo, A. Hollmann, N.C. Santos, Effect of 25-hydroxycholesterol in viral membrane fusion: insights on HIV inhibition, Biochim. Biophys. Acta Biomembr. 1860 (2018) 1171–1178, https://doi.org/10.1016/j.bbamem.2018.02.001.
[30] J. Zhao, J. Chen, M. Li, M. Chen, C. Sun, Multifaceted functions of CH25H and 25HC to modulate the lipid metabolism, immune responses, and broadly antiviral activities, Viruses 12 (2020), https://doi.org/10.3390/v12070727.
[31] J. Zhang, G. Yang, X. Wang, Y. Zhu, J. Wang, 25-Hydroxycholesterol mediates cholesterol metabolism to restrict porcine deltacoronavirus infection via suppression of transforming growth factor β1, Microbiol. Spectr. 10 (2022) e0219822, https://doi.org/10.1128/spectrum.02198-22.
[32] G. Roos, T. Leanderson, E. Lundgren, Interferon-induced cell cycle changes in human hematopoietic cell lines and fresh leukemic cells, Cancer Res. 44 (1984) 2358–2362.
[33] D. Lundblad, E. Lundgren, Block of glioma cell line in S by interferon, Int. J. Cancer 27 (1981) 749–754, https://doi.org/10.1002/ijc.2910270604.
[34] F. Balkwill, J. Taylor-Papadimitriou, Interferon affects both G1 and S+G2 in cells stimulated from quiescence to growth, Nature 274 (1978) 798–800, https://doi.org/10.1038/274798a0.
[35] J.A. Kim, C. Åberg, A. Salvati, K.A. Dawson, Role of cell cycle on the cellular uptake and dilution of nanoparticles in a cell population, Nat. Nanotechnol. 7 (2011) 62–68, https://doi.org/10.1038/NNANO.2011.191.
[36] M.L. Buckley, D.P. Ramji, The influence of dysfunctional signaling and lipid homeostasis in mediating the inflammatory responses during atherosclerosis, Biochim. Biophys. Acta Mol. Basis Dis. 1852 (2015) 1498–1510, https://doi.org/10.1016/j.bbadis.2015.04.011.
[37] L.S. Davis, J. Hutcheson, C. Mohan, The role of cytokines in the pathogenesis and treatment of systemic lupus erythematosus, J. Interferon Cytokine Res. 31 (2011) 781–789, https://doi.org/10.1089/jir.2011.0047.
[38] V. Lecureur, E. Le Ferrec, M. N'diaye, M. Le Vee, C. Gardyn, D. Gilot, O. Fardel, ERK-dependent induction of TNFalpha expression by the environmental contaminant benzo(a)pyrene in primary human macrophages, FEBS Lett. 579 (2005) 1904–1910, https://doi.org/10.1016/j.febslet.2005.01.081.
[39] J.-Y. Min, Y.J. Jang, Macrolide therapy in respiratory viral infections, Mediat. Inflamm. 2012 (2012) 649570, https://doi.org/10.1155/2012/649570.
[40] L. Pacifico, L. Di Renzo, C. Anania, J.F. Osborn, F. Ippoliti, E. Schiavo, C. Chiesa, Increased T-helper interferon-gamma-secreting cells in obese children, Eur. J. Endocrinol. 154 (2006) 691–697, https://doi.org/10.1530/eje.1.02138.
[41] Q. Wang, M. Yang, C. Wang, J. Cui, X. Li, C. Wang, Diagnostic efficacy of serum cytokines and chemokines in fungal bloodstream infection in febrile patients, J. Clin. Lab. Anal. 34 (2020) e23149, https://doi.org/10.1002/jcla.23149.
[42] A.M. Bentley, Q. Hamid, D.S. Robinson, E. Schotman, Q. Meng, B. Assoufi, A. B. Kay, S.R. Durham, Prednisolone treatment in asthma. Reduction in the numbers of eosinophils, T cells, tryptase-only positive mast cells, and modulation of IL-4, IL-5, and interferon-gamma cytokine gene expression within the bronchial mucosa, Am. J. Respir. Crit. Care Med. 153 (1996) 551–556, https://doi.org/10.1164/ajrccm.153.2.8564096.
[43] C.H.T. Miller, S.G. Maher, H.A. Young, Clinical use of interferon-gamma, Ann. N. Y. Acad. Sci. 1182 (2009) 69–79, https://doi.org/10.1111/j.1749-6632.2009.05069.x.
[44] K. Katayama, A. Kasahara, Y. Sasaki, T. Kashiwagi, M. Naito, M. Masuzawa, M. Katoh, H. Yoshihara, T. Kamada, T. Mukuda, T. Hijioka, M. Hori, N. Hayashi, Immunological response to interferon-gamma priming prior to interferon-alpha treatment in refractory chronic hepatitis C in relation to viral clearance, J. Viral Hepat. 8 (2001) 180–185, https://doi.org/10.1046/j.1365-2893.2001.00274.x.
[45] J. Wang, R. Oberley-Deegan, S. Wang, M. Nikrad, C.J. Funk, K.L. Hartshorn, R. J. Mason, Differentiated human alveolar type II cells secrete antiviral IL-29 (IFN-lambda 1) in response to influenza A infection, J. Immunol. 182 (2009) 1296–1304, https://doi.org/10.4049/jimmunol.182.3.1296.
[46] R.T. Bailer, B. Lee, L.J. Montaner, IL-13 and TNF-α inhibit dual-tropic HIV-1 in primary macrophages by reduction of surface expression of CD4, chemokine receptors CCR5, CXCR4 and post-entry viral gene expression, Eur. J. Immunol. 30 (2000) 1340–1349, https://doi.org/10.1002/(SICI)1521-4141(200005)30:5<1340:AID-IMMU1340>3.0.CO;2-L.
[47] M. Mordstein, G. Kochs, L. Dumoutier, J.-C. Renauld, S.R. Paludan, K. Klucher, P. Staeheli, Interferon-lambda contributes to innate immunity of mice against influenza A virus but not against hepatotropic viruses, PLoS Pathog. 4 (2008) e1000151, https://doi.org/10.1371/journal.ppat.1000151.
[48] T. Vincent, R.F. Pettersson, R.G. Crystal, P.L. Leopold, Cytokine-mediated downregulation of coxsackievirus-adenovirus receptor in endothelial cells, J. Virol. 78 (2004) 8047–8058, https://doi.org/10.1128/JVI.78.15.8047-8058.2004.
[49] S.G. Tilden, M.H. Ricco, E.A. Hemann, T.J. Anchordoquy, Reducing off-target drug accumulation by exploiting a type-III interferon response, J. Contr. Release 358 (2023) 729–738, https://doi.org/10.1016/j.jconrel.2023.05.029.
[50] R. Karki, B.R. Sharma, S. Tuladhar, E.P. Williams, L. Zalduondo, P. Samir, M. Zheng, B. Sundaram, B. Banoth, R.K.S. Malireddi, P. Schreiner, G. Neale, P. Vogel, R. Webby, C.B. Jonsson, T.-D. Kanneganti, Synergism of TNF-α and IFN-γ triggers inflammatory cell death, tissue damage, and mortality in SARS-CoV-2 infection and cytokine shock syndromes, Cell 184 (2021) 149–168.e17, https://doi.org/10.1016/j.cell.2020.11.025.
[51] O. Zimmer, A. Goepferich, How clathrin-coated pits control nanoparticle avidity for cells, Nanoscale Horiz 8 (2023) 256–269, https://doi.org/10.1039/d2nh00543c.
[52] M. Bohley, A.E. Dillinger, F. Schweda, A. Ohlmann, B.M. Braunger, E.R. Tamm, A. Goepferich, A single intravenous injection of cyclosporin A-loaded lipid nanocapsules prevents retinopathy of prematurity, Sci. Adv. 8 (2022) eabo6638, https://doi.org/10.1126/sciadv.abo6638.
[53] S. Mahammad, I. Parmryd, Cholesterol depletion using methyl-β-cyclodextrin, Methods Mol. Biol. 1232 (2015) 91–102, https://doi.org/10.1007/978-1-4939-1752-5_8.
[54] D.F. Gilbert, O. Friedrich (Eds.), Cell Viability Assays: Methods and Protocols, Springer New York, New York, NY, 2017. Imprint; Humana Press.
[55] D. Sladowski, S.J. Steer, R.H. Clothier, M. Balls, An improved MTT assay, J. Immunol. Methods 157 (1993) 203–207, https://doi.org/10.1016/0022-1759(93)90088-o.
[56] M.J. Stoddart (Ed.), Mammalian Cell Viability: Methods and Protocols, Humana Press, Totowa (N.J.), 2011.